Ab Initio Prediction of Vibrational Absorption and Circular Dichroism Spectra of Chiral Natural Products Using Density Functional Theory: α-Pinene

F. J. Devlin and P. J. Stephens*

Department of Chemistry, University of Southern California, Los Angeles, California 90089-0482

J. R. Cheeseman and M. J. Frisch

Lorentzian Inc., 140 Washington Avenue, North Haven, Connecticut 06473

Received: June 11, 1997; In Final Form: October 15, 1997[⊗]

Ab initio density functional theory (DFT) is used to analyze the vibrational unpolarized absorption and circular dichroism spectra of the chiral monoterpene, α-pinene. Large (TZ2P) basis set calculations using the hybrid functionals B3PW91 and B3LYP are in excellent overall agreement with experiment and permit the assignment of a large fraction of the fundamental frequencies. The quantitative accuracy of DFT in predicting the frequencies, dipole strengths, and rotational strengths of the fundamentals of α-pinene is documented for the B3PW91 and B3LYP functionals at both TZ2P and 6-31G* basis set levels. Hartree−Fock/self-consistent field (HF/SCF) calculations have also been carried out in parallel. The accuracy of the HF/SCF methodology is markedly inferior to that of DFT. In particular, HF/SCF predictions of the vibrational circular dichroism (VCD) spectrum of α-pinene are in very poor agreement with experiment.

Introduction

The first measurements of vibrational circular dichroism (VCD) in the chiral monoterpene, α-pinene (**1**) were reported more than 20 years ago.[1] Measurements were limited to the

(1*R*)-(+)-**1**

C−H stretching spectral region. The VCD of α-pinene was weak and barely detectable. Since that time, VCD instrumentation has improved enormously in sensitivity and frequency range.[2,3] As a result, measurement of VCD is now relatively straightforward across a considerable fraction of the fundamental vibrational infrared spectral region. The lower frequency limit is currently ∼700 cm^{-1}.[4] As developments in VCD instrumentation have occurred, α-pinene has frequently been used to assess instrumental sensitivity and the magnitude of polarization artifacts. A substantial number of VCD spectra are therefore to be found in the literature.[1−30] As time has passed, the VCD spectrum of α-pinene has become increasingly well-defined.

Despite the attention the VCD of α-pinene has received experimentally, its theoretical analysis has been virtually ignored.[31] The successful prediction of the VCD spectrum of a molecule of the size and complexity of α-pinene has not been practicable. However, very recently there have been major methodological advances which now permit calculations on α-pinene of useful accuracy. Specifically, new methods for predicting vibrational frequencies and rotational strengths using ab initio density functional theory (DFT) permit calculations of VCD spectra both more accurately and more efficiently than heretofore.[32−34] The primary purpose of this paper is to utilize these new methods in analyzing the VCD spectrum—and, simultaneously, the unpolarized absorption spectrum—of α-pinene. We also take this opportunity to report previously unpublished VCD spectra, measured using the USC dispersive spectrometer.[1,4,5]

Methods

Unpolarized absorption spectra were measured at 1 cm^{-1} resolution using a Nicolet MX1 FTIR spectrometer.

VCD was measured using a dispersive instrument.[1,4,5] Substantial changes were made to this instrumentation since last described, resulting in significant improvements in sensitivity. The current configuration is as follows.

Light from a carbon rod source is focused by two mirrors to form a 1:1 image at the entrance slit of the monochromator. A mechanical chopper, placed before the entrance slit, modulates the light beam at a frequency ω_c. An interference filter, placed after the monochromator, removes higher orders from the diffracted beam, which is then linearly polarized and passed through a photoelastic modulator, operating at a frequency ω_m. After passage through the sample cell, the modulated beam is focused by a lens onto a cooled infrared detector.

The carbon rod source is operated at 8.3 V and 220 A (1.8 kW) from an ac power supply giving a color temperature of ∼2400 K. The rod (General Graphites) is 6 in. long and $^1/_4$ in. in diameter with the center 1-$^1/_4$ in. machined down to a semicircular cross section. It is mounted in a water-cooled housing equipped with a CaF_2 or KCl window and filled with argon (1 atm). The rod lifetime is typically 100−200 h. The variable frequency chopper (Ithaco, Inc., Model 220) is operated at 275 Hz.

The computer-controlled $^3/_4$ m Czerny-Turner f/6.8 monochromator (Spex, Model 1500SP) is evacuated and equipped with entrance and exit windows of CaF_2 or KCl. The maximum slit width is 3 mm. Bausch and Lomb gratings (102 × 102 mm) blazed at 3.0, 4.65, 10.0, and 10.0 μm (300, 75, 75, and

* To whom correspondence should be addressed.
[⊗] Abstract published in *Advance ACS Abstracts,* December 1, 1997.

S1089-5639(97)01905-1 CCC: $14.00

25 g/mm, respectively) are used in first order and span the 2−15 μm region. Radiation higher than first order is removed by using long-wave-pass interference filters with cut-on at 2.3, 3.1, 4.8, and 8.2 μm (L02288-9, LO3052-8, LO4840-9, and LO8154-9, respectively; OCLI Inc.) on either germanium or silicon substrates. Grating/filter changes are chosen so as to optimize the light throughput of the instrument.

Linear polarization is achieved using an aluminum grid deposited on either BaF_2 (Cambridge Physical Sciences, Model IGP 228) or ZnSe (PTR Optics Corp., Model GP 200-25-00) substrates. The ZnSe polarizer has an extinction ratio of 100 at 3.0 μm and 1000 at 10.0 μm; the BaF_2 polarizer has a somewhat lower extinction ratio, but over its usable range it has higher transmission.

Phase modulation is carried out using photoelastic modulators with octagonal optical elements of CaF_2 or ZnSe operating at 60 and 39 kHz, respectively (Hinds Intl., JCK-Series). The ZnSe element is AR coated for 10.6 μm. These modulators provide greater than $\lambda/4$ peak retardation to their transmission limits ($\approx$8 μm for CaF_2 and $\approx$16 μm for ZnSe). The modulator power supply is synchronized to the monochromator; as the latter is scanned, a constant level of phase modulation is maintained.

After the modulated beam traverses the sample, it is focused onto the detector by a f/1.7 CaF_2 or f/1 ZnSe (Janos Technology Inc.) lens. Cooled semiconductor detectors (Santa Barbara Research Center) are used; specific detectors are: 1 mm diameter photovoltaic InSb ($D^*_{\lambda_{max}} = 1.4 \times 10^{11}$, $\lambda_{max} = 5$ μm) cooled to 30 K, 1 mm × 1 mm photoconductive HgCdTe ($D^*_{\lambda_{max}} = 4 \times 10^{10}$, $\lambda_{max} = 12.0-13.5$ μm) cooled to 77 K and 1 mm diameter extrinsic Si:As photoconductor ($D^*_{\lambda_{max}} = 3.3 \times 10^{10}$, $\lambda_{max} = 23$ μm) operating at 12 K. They are mounted in a modified, vibration-isolated, cold head (Laser Analytics Inc., Model TCR), which is interfaced to a closed-cycle refrigerator (CTI-Cryogenics, Model 21). Temperature regulation is provided by a proportional/integral controller (Laser Analytics Inc., Model CTS) employing a silicon diode temperature sensor. The refrigerator window is 2 mm thick CaF_2 or AR coated ZnSe. A cooled 30° field-of-view shield is placed directly in front of the detector inside the refrigerator.

The detector signal contains components at frequencies ω_c and ω_m. After preamplification, the detector signal is fed to an automatic normalization circuit which amplifies or attenuates both the ω_c and ω_m signals equally, so that the ω_c component is held at a constant level. The output of the normalization circuit is passed through a tuned filter into a lock-in amplifier tuned to ω_m whose output varies at ω_c. Subsequent demodulation by a lock-in amplifier tuned to ω_c yields a dc signal which is proportional to the sample VCD, ΔA.[5] Single-beam absorption spectra can also be obtained by sending the preamplified signal directly to the lock-in amplifier tuned to ω_c.

The preamplifier is mounted close to the closed-cycle refrigerator and is well-shielded to avoid noise from the refrigerator system. In the case of photovoltaic detectors a low-noise current-to-voltage converter (Analog Devices, Model 48K) is used, which maintains the detector at zero bias voltage where its detectivity is a maximum. With photoconductive elements, a bias circuit with a suitable load resistor is used and the detector signal ac coupled to a noninverting amplifier (Analog Devices, Model 45K).

Normalization is achieved by means of a servoamplifier and a photoattenuator (Raytheon, Model CK1116). The attenuator serves as the variable portion of a resistor network across which the preamplifier signal is applied. Inclusion of a lock-in amplifier (Princeton Applied Research, Model 122) in the feedback loop, referenced to ω_c, ensures that the input to the servoamplifier is limited to the ω_c component of the signal.

The VCD signal is demodulated at ω_m by a lock-in amplifier (PAR 124 A) operating in a band-pass mode with a Q of 100, a high dynamic reserve, and a low time constant (<1 ms) with a 6 dB/oct roll-off rate to ensure passage of the 275 Hz modulated signal. A tuned LC filter, whose center frequency is matched to ω_m, precedes the PAR 124A to prevent the large ω_c signal from overloading the amplifier. The output of this lock-in is further demodulated by a heterodyning amplifier (PAR 186A), tuned to 275 Hz. The use of two lock-in amplifiers in series discriminates against ground loops and other stray signals at ω_m.

Calibration spectra[5] are obtained with two orientations of a birefringent plate and polarizer unit different by $\pi/2$. For $\lambda <$ 6 μm the calibration unit consists of a sapphire plate and a grid polarizer on a ZnSe substrate; for longer wavelengths a CdSe plate (Cleveland Crystals Inc.) is used.

VCD spectra were measured for each enantiomer of **1**. Base lines were obtained using racemic **1**. All samples of **1** were obtained from Aldrich and used without further purification. Specified purities and specific rotations were: (+), 99+% and $[\alpha]^{21} = +50.7°$; (−), 99% and $[\alpha]_D^{20} = -50.7°$; (±), 98%. Using $[\alpha]_D^{20} = 51.60°$ for optically pure (+)-**1**,[35] the enantiomeric excesses (ee) of (+)-**1** and (−)-**1** used here were 98.3% and 98.3%, respectively. Final VCD spectra were obtained by normalizing the spectra of (+)-**1** and (−)-**1** to 100% ee and then taking one half of the difference of the two spectra. One half of the sum of the two spectra indicates the degree to which the spectra are equal and opposite in magnitude and sign respectively.

Absorption and VCD spectra of **1** were fit, using the equations[36,37]

$$\epsilon(\bar{\nu}) = \frac{8\pi^3 N}{3000hc(2.303)}\bar{\nu}\sum_i \mathrm{D}_i \mathrm{f}_i(\bar{\nu},\bar{\nu}_i) \tag{1}$$

$$\Delta\epsilon(\bar{\nu}) = \frac{32\pi^3 N}{3000hc(2.303)}\bar{\nu}\sum_i \mathrm{R}_i \mathrm{f}_i(\bar{\nu},\bar{\nu}_i) \tag{2}$$

where $\bar{\nu}_i$, D_i, and R_i are excitation frequencies, dipole strengths, and rotational strengths. The normalized band shape, $f_i(\bar{\nu},\bar{\nu}_i)$ is assumed to be Lorentzian:

$$f_i(\bar{\nu},\bar{\nu}_i) = \frac{1}{\pi\gamma_i}\frac{\gamma_i}{[(\bar{\nu}-\bar{\nu}_i)^2+\gamma_i^2]} \tag{3}$$

where γ_i is the half-width at half-height. Fitting was carried out using the Peak Fit program (Jandel Scientific Software).

Ab initio calculations of the frequencies, dipole strengths, and rotational strengths of **1** were carried out within the harmonic approximation using the equations[38,39]

$$D_i = |\langle 0|\boldsymbol{\mu}_{el}|1\rangle_i|^2 \tag{4}$$

$$R_i = \mathrm{Im}[\langle 0|\boldsymbol{\mu}_{el}|1\rangle_i \cdot \langle 1|\boldsymbol{\mu}_{mag}|0\rangle_i] \tag{5}$$

$$\langle 0|(\mu_{el})_\beta|1\rangle_i = \left(\frac{\hbar}{2\omega_i}\right)^{1/2}\sum_{\lambda\alpha} S_{\lambda\alpha,i}P^\lambda_{\alpha\beta} \tag{6}$$

$$\langle 0|(\mu_{mag})_\beta|1\rangle_i = -(2\hbar^3\omega_i)^{1/2}\sum_{\lambda\alpha} S_{\lambda\alpha,i}M^\lambda_{\alpha\beta} \tag{7}$$

Here, $\hbar\omega_i = hc\bar{\nu}_i$ is the excitation energy of the ith fundamental,

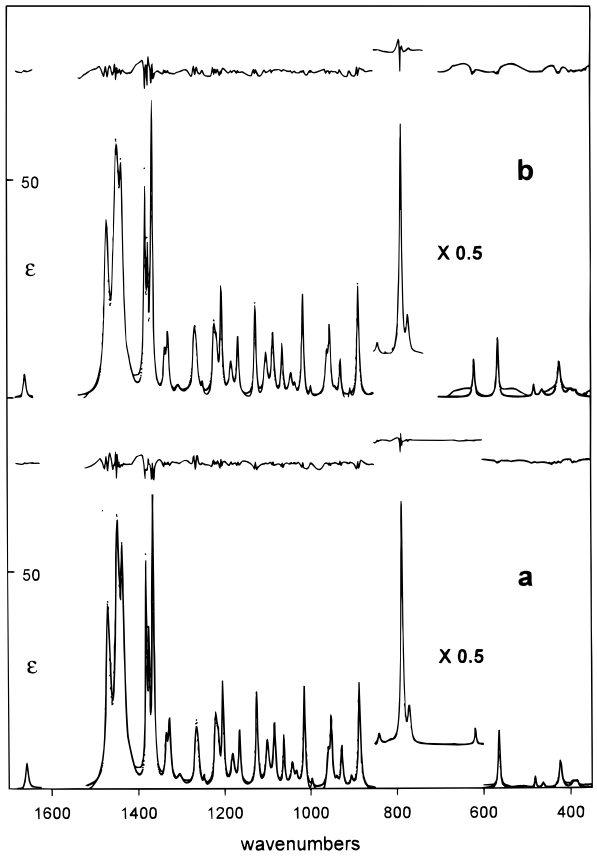

Figure 1. Mid-IR unpolarized absorption spectra of (*S*)-(−)- **1**: (a) 0.49 M CCl_4 solution, 1680−350 cm^{-1} (inset is for 0.49 M CS_2 solution, 850−600 cm^{-1}); (b) neat liquid, 1680−350 cm^{-1}. Resolution is 1 cm^{-1}. Solid lines are experimental spectra; dotted lines are Lorentzian fits. Difference spectra (experiment − fit) are also shown (solid lines above spectra).

$P^{\lambda}_{\alpha\beta}$ and $M^{\lambda}_{\alpha\beta}$ are the atomic polar tensors (APTs) and atomic axial tensors (AATs),[39,40] respectively, and the $S_{\lambda\alpha,i}$ matrix converts Cartesian displacement coordinates, $X_{\lambda\alpha}$, to normal coordinates, Q_i,

$$X_{\lambda\alpha} = \sum_i S_{\lambda\alpha,i} Q_i \tag{8}$$

$S_{\lambda\alpha,i}$ and ω_i are obtained simultaneously by diagonalization of the mass-weighted Cartesian harmonic force field (HFF) (the Hessian).

DFT HFFs, APTs, and AATs of **1** were calculated using direct, analytical derivative methods implemented within the GAUSSIAN program[41] as described previously.[32,42−46] In this work the hybrid functionals B3PW91 and B3LYP have been used. B3PW91 is the functional of Becke.[47] B3LYP is a subsequent functional also incorporated in the GAUSSIAN program.[42,43] All DFT calculations use the "fine" grid.[42,43]

HFFs, APTs, and AATs were also calculated at the Hartree−Fock/self-consistent field (HF/SCF) level of approximation, again using direct, analytical derivative methods and the GAUSSIAN program.[32]

Both DFT and HF/SCF AATs are calculated using GIAO basis sets.[32,44,48,49] Accordingly, AATs are gauge-independent (common origin gauge and distributed origin gauge AATs[39,40] are identical), and common origin gauge AATs yield origin-independent rotational strengths.

Calculations use the 6-31G*[50] and TZ2P[40] basis sets. For **1** calculations using these [3s2p1d/2s] and [5s4p2d/3s2p] basis sets involve 182 and 434 basis functions, respectively.

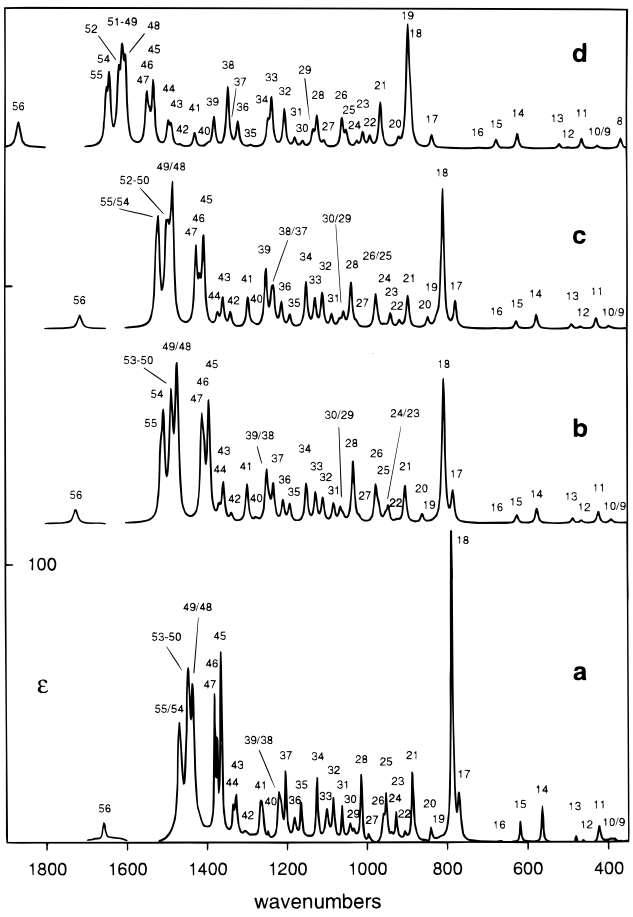

Figure 2. Experimental (a) and calculated (b−d) mid-IR absorption spectra of **1**. The experimental spectrum is from Figure 1a (CCl_4 solution data at >850 and <600 cm^{-1}; CS_2 solution data for 850−600 cm^{-1}). Calculated spectra are (b) DFT/B3PW91/TZ2P; (c) DFT/B3LYP/TZ2P; (d) HF/SCF/TZ2P. $\gamma = 4$ cm^{-1} for all bands in (b−d). Numbers indicate fundamentals.

Ab initio calculations were carried out using Silicon Graphics Power Challenge and IBM SP2 machines.

Results

Unpolarized absorption spectra at 1 cm^{-1} resolution of **1** over the frequency range 1680−350 cm^{-1} are shown in Figure 1. Spectra have been obtained for the neat liquid and for CCl_4 and CS_2 solutions. Figure 1 shows the neat liquid and CCl_4 solution spectra; in the region of strongest CCl_4 absorption the CS_2 solution spectrum is also shown. The neat liquid and solution spectra are very similar, demonstrating the absence of substantial concentration effects in the neat liquid spectrum.

The frequencies and dipole strengths predicted for **1** using DFT, the B3PW91 functional, and the TZ2P basis set are given in Table 1. The absorption spectrum predicted thence, using Lorentzian band shapes ($\gamma = 4$ cm^{-1}) over the range 1800−350 cm^{-1} is shown in Figure 2. Allowing for the expected small shift to higher frequency,[51] the calculated spectrum is in excellent overall qualitative agreement with the experimental spectrum, also shown in Figure 2. Assignment of a large majority of fundamentals 9−56 follows straightforwardly. Modes 9−47 and 56 are clearly identifiable in the experimental spectrum, as indicated in Figure 2. Modes 48−55 are not fully resolved; however, the predicted triplet structure in this region is in qualitative agreement with the experimental spectrum.

Quantitative analysis of the experimental absorption spectrum of **1**, guided by the above qualitative assignment, is carried out by Lorentzian fitting. The fits for both solution and neat liquid

TABLE 1: TZ2P Calculations for α-Pinene (1)[a]

	DFT								
	B3PW91			B3LYP			HF/SCF		
mode	ν	D	R	ν	D	R	ν	D	R
72	3156	24.8	−0.2	3149	26.2	0.0	3299	31.8	0.0
71	3136	45.8	2.7	3127	51.4	3.0	3275	87.6	5.5
70	3133	12.3	1.7	3124	12.9	1.0	3274	13.1	−1.7
69	3120	31.5	0.1	3107	33.2	−0.9	3245	44.2	−1.6
68	3113	22.7	0.0	3097	25.1	1.1	3233	36.3	0.5
67	3092	48.1	−7.2	3076	55.1	−1.2	3215	41.4	−1.6
66	3086	4.6	0.6	3071	38.2	−17.2	3208	112.8	−18.3
65	3078	40.0	−10.4	3068	4.7	−0.1	3200	44.0	−0.5
64	3068	56.0	2.2	3060	52.9	1.2	3194	7.0	8.6
63	3066	17.1	−1.1	3048	34.7	2.2	3188	50.9	3.0
62	3058	63.2	0.6	3048	58.6	−0.9	3188	81.4	−5.7
61	3033	69.6	9.2	3027	65.2	4.3	3165	59.1	13.2
60	3031	17.0	−4.9	3020	21.9	−2.3	3162	66.8	−8.1
59	3027	21.8	0.6	3017	24.5	4.2	3152	20.9	1.1
58	3016	35.6	−2.2	3009	35.6	−2.0	3148	37.8	−3.9
57	3007	46.4	3.9	2999	47.9	4.1	3145	65.6	6.5
56	1725	5.0	1.0	1714	4.8	1.0	1867	8.4	1.1
55	1513	16.0	0.4	1523	15.2	1.1	1648	11.3	6.4
54	1506	24.6	−1.1	1518	23.5	−0.7	1640	15.8	−4.0
53	1493	5.2	2.2	1504	2.8	1.5	1624	0.3	0.2
52	1487	25.5	0.6	1498	18.5	−0.5	1618	14.7	0.8
51	1483	8.9	0.4	1493	13.5	1.5	1611	9.3	−0.4
50	1476	8.0	1.3	1488	10.3	0.8	1608	8.2	2.5
49	1473	24.0	−0.8	1483	12.3	0.8	1606	7.2	−0.7
48	1471	16.5	0.5	1482	22.1	−1.3	1600	17.8	−0.8
47	1411	25.5	−2.2	1424	21.3	−2.0	1547	12.5	−1.4
46	1405	14.0	−0.9	1415	8.8	−1.0	1541	4.8	−1.0
45	1393	33.4	−1.1	1405	25.1	−0.3	1531	16.7	−2.6
44	1368	3.5	−1.7	1370	3.6	−2.0	1494	6.0	0.3
43	1357	11.2	9.7	1357	8.6	7.1	1486	5.2	7.7
42	1337	2.3	2.1	1338	4.4	3.0	1464	0.5	−0.7
41	1298	12.1	−4.6	1294	9.6	−5.2	1428	4.2	−3.7
40	1275	1.1	−0.7	1280	0.8	−1.4	1394	0.8	−1.2
39	1249	16.1	−1.7	1249	18.6	−1.6	1379	8.9	−4.5
38	1241	4.2	−12.4	1235	8.3	−7.0	1345	18.3	−2.8
37	1232	11.7	−3.3	1230	9.3	−2.3	1335	0.5	0.0
36	1207	7.1	3.4	1210	8.2	0.6	1320	7.8	3.9
35	1191	6.0	0.6	1190	4.1	−1.5	1288	0.6	−3.5
34	1149	13.7	14.7	1148	16.2	15.3	1244	7.2	−2.5
33	1126	10.6	−15.3	1126	10.1	−14.4	1235	15.7	2.4
32	1108	8.8	2.2	1108	12.4	3.4	1203	13.1	5.5
31	1081	6.9	−10.6	1085	4.9	−5.5	1177	3.1	−6.5
30	1064	5.0	5.0	1065	2.6	−2.6	1158	2.1	−4.8
29	1058	2.3	−1.1	1055	5.4	2.8	1131	5.1	−1.4
28	1032	24.3	19.1	1036	17.9	15.8	1121	11.1	11.0
27	1017	1.7	−14.9	1023	1.7	−14.2	1104	2.2	−13.3
26	975	14.9	−9.8	975	12.3	−6.3	1058	11.1	6.5
25	968	5.0	1.3	971	3.9	2.0	1048	5.6	0.0
24	952	2.6	1.0	953	1.1	−0.8	1022	2.2	−2.4
23	944	6.7	6.8	938	6.3	2.2	1007	6.1	0.6
22	922	0.9	2.8	916	3.1	5.9	989	4.6	6.0
21	902	16.9	0.3	895	14.9	−1.0	963	19.5	−2.4
20	859	4.0	5.1	845	4.8	4.5	918	3.4	8.0
19	831	0.4	2.8	823	2.5	3.0	895	52.3	3.9
18	806	74.2	−1.7	808	71.6	−1.8	888	19.9	−2.7
17	783	15.5	7.7	777	13.7	7.7	834	6.3	3.5
16	676	0.3	1.3	672	0.3	1.2	718	0.4	0.9
15	624	5.5	−7.4	625	5.1	−6.4	674	5.5	−6.0
14	575	10.4	4.0	575	10.0	3.0	622	9.8	3.2
13	486	4.2	−4.1	488	3.9	−3.6	518	3.6	−3.1
12	464	2.6	0.0	467	1.8	0.2	497	0.7	−0.6
11	423	11.0	0.4	427	10.4	0.3	463	8.7	0.2
10	391	3.8	−0.2	397	2.5	0.1	424	2.7	0.1
9	387	0.8	0.6	391	1.2	0.5	420	0.4	0.7
8	330	15.6	−5.3	332	13.9	−4.9	365	11.6	−4.2
7	304	12.8	−7.1	306	12.4	−6.7	326	8.6	−5.1
6	259	0.7	1.9	261	0.6	1.5	279	0.3	0.8
5	227	4.0	5.0	227	3.8	4.9	243	4.3	5.0
4	205	3.4	−0.4	206	3.0	−0.3	221	1.7	0.0
3	195	1.5	−1.0	196	1.4	−1.0	208	1.8	−0.4
2	186	1.7	3.6	185	1.5	3.3	182	1.8	3.6
1	128	32.7	−2.3	127	31.5	−2.3	136	29.9	−2.4

[a] ν in cm^{-1}, D in 10^{-40} esu^2 cm^2, R in 10^{-44} esu^2 cm^2. Rotational strengths are for the R-(+) enantiomer.

TABLE 2: Experimental Parameters for α-Pinene (1)[a]

	absorption						VCD[c]					
	soln			neat			disp.[d]			FT[e]		
mode[b]	ν	D	γ	ν	D	γ	ν	R	γ	ν	R	γ
56	1658	3.5	3.4	1659	2.7	3.0						
55	1471	15.8	4.5	1471	16.2	4.6				1474	−3.3	4.1
54	1468	23.4	4.7	1468	24.0	5.2				1468	4.1	3.7
53	1453	11.1	4.9	1453	14.1	5.0				1455	−0.6	2.8
52	1447	31.4	3.8	1448	27.9	4.0				1452	−0.3	2.7
51	1443	13.4	3.9	1443	16.6	3.8				1444	−0.5	2.3
50	1440	5.1	7.0	1440	7.0	6.7				1440	0.2	1.7
49	1436	25.5	3.6	1436	24.2	3.9				1435	0.5	1.7
48	1433	11.9	5.8	1432	13.3	5.5				1431	−0.4	1.8
	1418	7.6	9.6	1418	8.1	10.0						
47	1381	19.6	1.9	1381	19.4	2.0				1382	2.8	3.4
46	1375	10.6	1.8	1375	10.6	1.8				1374	1.2	3.0
45	1365	35.8	2.6	1365	35.8	2.6				1365	2.2	3.0
44	1336	6.2	3.2	1335	4.9	2.9	1336	−1.4	8.4	1333	−1.5	7.0
43	1328	11.2	3.7	1328	9.4	3.3	1329	11.7	5.5	1329	8.9	4.5
42	1304	3.6	6.8	1305	2.8	6.8	1306	0.2	4.0	1307	0.7	3.0
41	1265	15.0	4.3	1265	20.1	5.5	1263	−10.1	5.6	1265	−8.0	4.1
40	1248	0.6	1.6	1248	0.5	1.5	1247	−0.7	6.5	1258	−0.4	3.0
39	1221	12.6	3.7	1221	11.8	3.4	1224	4.2	4.6	1224	5.7	4.2
38	1215	6.7	3.4	1215	7.0	3.2	1213	−29.7	4.9	1215	−28.5	5.0
37	1204	13.6	2.5	1204	14.3	2.5	1200	2.5	3.5	1201	1.3	2.6
36	1182	8.0	4.7	1181	7.9	4.5	1181	8.9	5.0	1183	7.6	5.0
35	1165	8.7	2.8	1165	9.0	2.8	1165	1.8	3.4	1167	1.3	3.8
34	1125	16.6	3.0	1125	13.0	2.4	1125	24.2	4.4	1126	16.7	4.0
33	1101	12.1	4.5	1100	10.4	4.3	1100	−25.7	5.0	1102	−21.1	4.9
32	1084	12.1	3.3	1084	12.1	3.3	1084	−0.3	6.8	1085	−0.7	3.0
31	1063	7.2	2.3	1063	7.2	2.3	1062	−13.6	4.3	1064	−8.9	3.4
30	1043	6.4	4.5	1043	6.0	4.5	1041	6.3	5.0	1043	4.8	5.3
29	1033	2.3	3.2	1033	1.3	2.4	1032	−0.9	4.2	1034	−0.3	3.2
28	1015	17.8	2.7	1015	17.4	2.6	1014	14.7	4.0	1015	10.6	4.5
27	997	0.7	1.6	996	0.7	1.3	996	−28.3	4.4	997	−19.3	3.7
26	959	6.6	3.2	959	8.4	3.3	959	−8.6	4.6	959	−6.0	4.2
25	952	13.4	2.9	952	13.2	2.9	950	4.2	3.7	952	2.8	3.8
24	939	1.3	2.9	940	0.8	2.2	939	−6.2	4.6	940	−3.8	4.4
23	928	8.0	2.8	928	6.1	2.5	926	3.3	3.4	928	3.6	4.6
22	906	2.1	3.0	905	0.3	0.7	905	5.2	2.2	906	7.4	3.9
21	887	23.7	3.0	886	22.7	2.7	886	4.5	2.1	888	4.1	2.6
20	841	5.3	3.2	842	5.3	3.3	841	5.2	2.1	842	9.0	4.6
19	815	3.5	7.8				820	1.0	1.9	821	3.3	3.7
18	787	108.1	2.6	787	98.0	2.5	784	−3.6	1.9			
17	771	20.5	3.5	771	20.3	3.5	768	14.5	5.3			
16	667											
15	619	7.1	2.0	619	10.0	2.5						
14	564	15.6	2.3	564	17.5	2.5						
13	481	3.0	2.0	481	3.5	2.2						
12	463	2.1	2.9	463	4.4	4.5						
11	423	16.3	3.9	423	24.5	4.5						
10	392	5.6	5.3	398	6.5	6.1						
9	384	2.9	3.4	386	4.6	4.9						

[a] From Lorentzian fitting to experimental absorption and VCD spectra (Figures 1 and 5); ν and γ in cm^{-1}, D in 10^{-40} esu^2 cm^2, R in 10^{-44} esu^2 cm^2. [b] Assignment. [c] For the *R*-(+) enantiomer. [d] From Lorentzian fitting to the dispersive VCD spectrum (Figure 5a). [e] From Lorentzian fitting to the FT spectrum (Figure 5b).

spectra are shown in Figure 1. Their accuracies are documented by the difference spectra (experimental spectrum−fit) also shown in Figure 1. The frequencies, dipole strengths, and bandwidths obtained are listed in Table 2, together with their assignments. All fundamentals 9−56 are assigned. The fits include only one band (between modes 47 and 48), which is assigned as a nonfundamental. In the case of the unresolved modes 48−55, the fits are obviously not unique and the frequencies and dipole strengths obtained are accordingly less reliable.

The frequencies and dipole strengths predicted for **1** using DFT, the B3LYP functional, and the TZ2P basis set are also given in Table 1. The absorption spectrum predicted thence over the range 1800−350 cm^{-1} is also shown in Figure 2. The spectra predicted using the B3LYP and B3PW91 functionals are qualitatively very similar. The B3LYP spectrum is in equally good qualitative agreement with experiment and leads to an identical assignment of fundamentals.

VCD spectra of neat liquid **1** over the frequency range 1350−750 cm^{-1} obtained using the USC dispersive spectrometer are shown in Figure 3. The VCD spectra of (+)-**1** and (−)-**1** are shown individually in Figure 3a. The spectrum of (+)-**1** obtained by differencing the two enantiomer spectra, thereby enhancing the signal-to-noise ratio, is shown in Figure 3b. The spectrum obtained by summing the two enantiomer spectra (Figure 3c) documents the noise and artifact levels in the VCD spectra. As expected, noise levels increase with decreasing frequency. Artefacts do not contribute significantly to the spectra. The dispersive VCD spectrum is also compared to data of Nafie and co-workers[2,52] measured using FT instrumentation in Figure 3b. Over the common frequency range, 815−1350

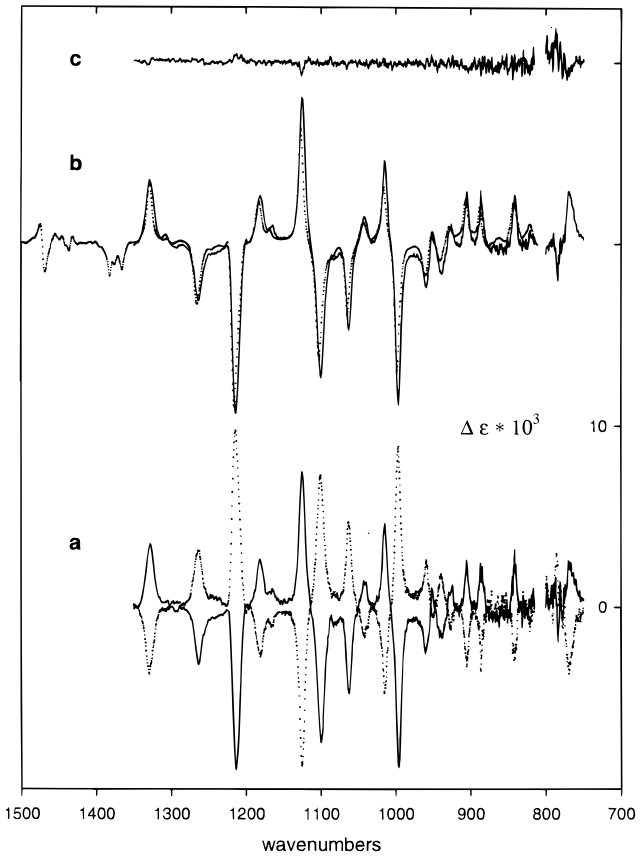

Figure 3. Mid-IR VCD of neat liquid **1**: (a) VCD spectra of (*R*)-(+)-**1** (solid line) and (*S*)-(−)-**1** (dotted line) (this work, except the spectra below 800 cm^{-1} which are taken from ref 4); (b) VCD spectrum of (*R*)-(+)-**1** obtained from the spectra of (+)-**1** and (−)-**1** in (a) (solid line); FT VCD data of Nafie and co-workers (refs 2 and 52) are superimposed (dotted line); (c) "noise spectrum", the average of the spectra of (+)-**1** and (−)-**1** in (a). The spectra in (a) were measured in sections: (i) 1350−1050 cm^{-1}, resolution 9.3−5.7 cm^{-1}; (ii) 1050−815 cm^{-1}, resolution 5.7−3.4 cm^{-1}; (iii) 800−750 cm^{-1}, resolution 9.9−8.6 cm^{-1}. The VCD spectra in (a) and (b) are normalized to 100% ee. In the case of the FT data from ref 2, path length and specific rotation were not reported and we have used 79 μm and 98.3% for these parameters. The former was obtained by comparing a 5 cm^{-1} resolution absorption spectrum using a known path length to the spectrum in ref 2.

cm^{-1}, the dispersive and FT spectra are qualitatively identical and quantitatively similar.

The rotational strengths predicted for **1** using DFT, B3PW91, and TZ2P are given in Table 1. The VCD spectrum predicted thence assuming Lorentzian bands of constant width ($\gamma = 4$ cm^{-1}) is shown in Figure 4, together with the experimental spectrum. VCD is clearly observed for the fundamentals 17−28, 30, 31, 33−36, 38, 41−43, 45−47, 54, and 55. Weak VCD is observed for the unresolved fundamentals 48−53. Modes 29, 32, 37, 39, 40, and 44 are not unambiguously observed. With the exception of modes 21−25 the calculated VCD spectrum is in excellent overall qualitative agreement with experiment, supporting the assignment arrived at from the absorption spectrum. In the case of modes 21−25 the agreement is significantly worse. Quantitative analysis of the VCD spectrum is carried out using Lorentzian fitting as shown in Figure 5 for both dispersive and FT data. The accuracy of the fits is shown by the difference spectra (experiment-fit). The frequencies, rotational strengths, and bandwidths obtained are given in Table 2. Note that since different spectrometers and resolutions are used in obtaining the absorption and VCD spectra, it is not possible to constrain either frequencies or

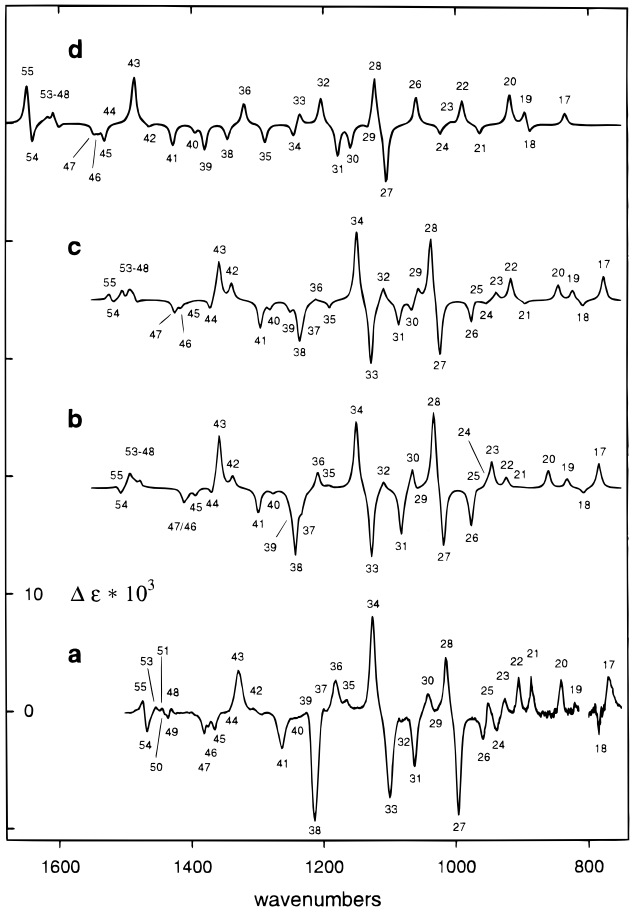

Figure 4. Experimental (a) and calculated (b−d) mid-IR VCD spectra of (*R*)-(+)-**1**. The experimental spectrum is from Figure 3b;. below 1350 cm^{-1} it is the dispersive spectrum; above 1350 cm^{-1} it is the FT spectrum. Calculated spectra are (b) DFT/B3PW91/TZ2P; (c) DFT/B3LYP/TZ2P; (d) HF/SCF/TZ2P. $\gamma = 4$ cm^{-1} for all bands in (b−d). Numbers indicate fundamentals.

bandwidths to be identical in the VCD and absorption spectra. As seen in Table 2, the frequency differences for corresponding bands are generally small and the bandwidths are generally greater for the VCD spectrum, as expected given its lower resolution. Rotational strengths are obtained for all fundamentals 17−55. In the case of the unresolved modes 48−55 the fit is obviously not unique and the rotational strengths obtained are accordingly less reliable.

The rotational strengths predicted using DFT, B3LYP, and TZ2P are also given in Table 1. The VCD spectrum predicted thence is also shown in Figure 4. Much of the spectrum is very similar to the B3PW91 spectrum. However, significant differences exist for modes 21−25, 29, 30, 35, and 48−53. In the case of modes 21−25 both B3PW91 and B3LYP spectra are in qualitative disagreement with experiment. In the case of modes 29, 30, and 35 the B3PW91 calculation is clearly superior. In the case of the unresolved modes 48−55 neither calculation is perfect, but neither is definitively superior. On balance, the B3PW91 calculation is overall in somewhat better qualitative agreement with experiment.

The quantitative agreement of calculated and experimental frequencies, dipole strengths, and rotational strengths for modes 9−56 is displayed in Figures 6−8. For both B3PW91 and B3LYP, calculated frequencies are greater than experimental frequencies, the percentage deviation increasing with frequency (Figure 6). The ranges of percentage deviations are −0.2 to 4.1% and 0.5 to 3.6% for B3PW91 and B3LYP, respectively. A significant fraction of the errors in calculated frequencies is

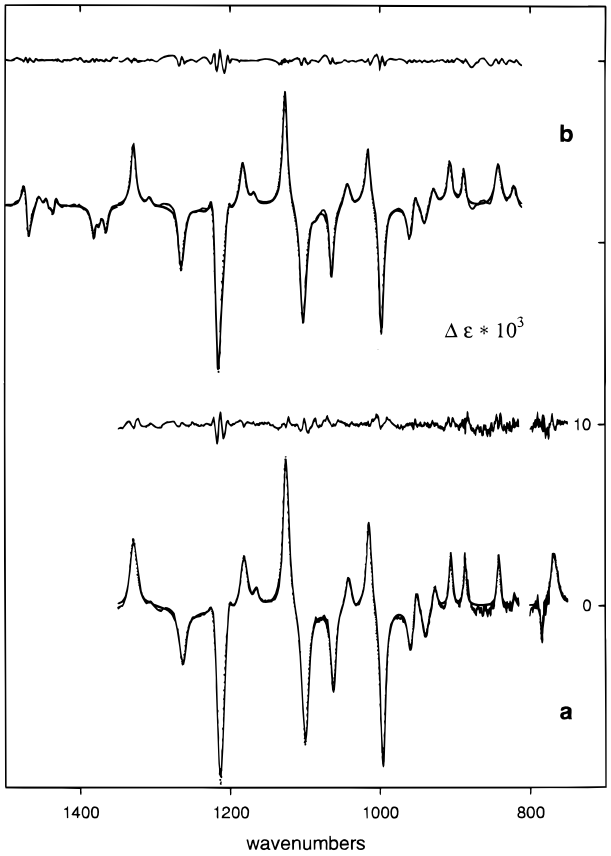

Figure 5. Lorentzian fits to experimental mid-IR VCD spectra: (a) dispersive spectrum; (b) FT spectrum, from refs 2 and 52. Solid lines are experimental spectra from Figure 3b; dotted lines are fits. Difference spectra (experiment − fit) are also shown (solid lines above spectra).

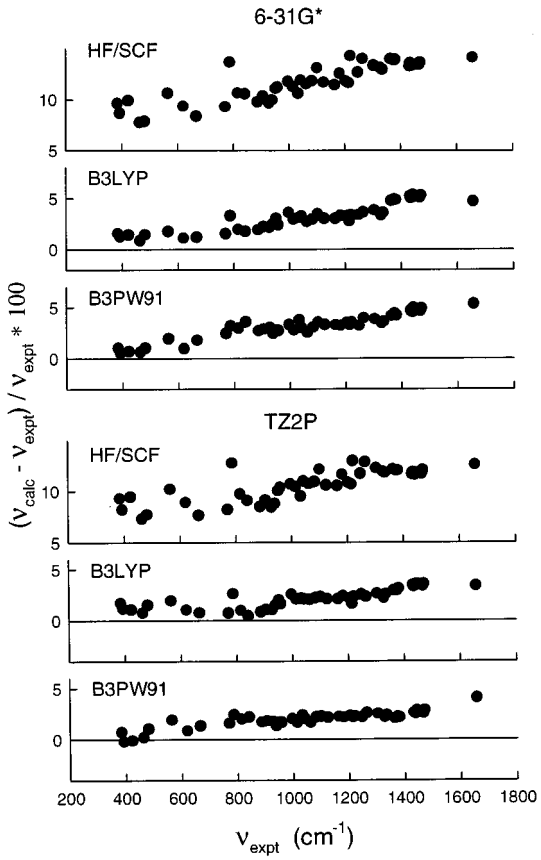

Figure 6. Comparison of calculated and experimental frequencies. The latter are solution values (Table 2).

attributable to the contributions of anharmonicity to the experimental frequencies. A study of a set of molecules for which harmonic frequencies have been obtained in addition to observed frequencies found, at the TZ2P basis set level, deviations of calculated harmonic frequencies from experimental harmonic frequencies averaging 1.2% for mid-IR modes.[51] The accuracy of the calculations on **1** is likely to be comparable.

Calculated B3PW91 and B3LYP dipole strengths are compared to experiment in Figure 7. Experimental dipole strengths have been obtained for both solutions (in CCl_4 and CS_2) of **1** and for neat liquid **1** (Table 2). The values obtained are compared in Figure 7. Calculated dipole strengths are compared to both sets of experimental dipole strengths. B3PW91 dipole strengths are in slightly better agreement with experiment than are B3LYP dipole strengths. There is little difference in the agreement for the two sets of experimental dipole strengths. That is, overall, the errors in calculated dipole strengths are significantly larger than the variations between solution and neat liquid dipole strengths. The errors in the calculated dipole strengths are attributable to errors in the harmonic calculation, anharmonicity, and condensed phase effects. The relative magnitudes of these errors are undefined at present.

Calculated B3PW91 and B3LYP rotational strengths are compared to experiment in Figure 8. Experimental rotational strengths have been obtained from both dispersive and FT data. The values obtained are compared in Figure 8. Calculated rotational strengths are compared to both sets of experimental rotational strengths. The B3PW91 and B3LYP calculations are in comparable agreement with experiment. There is not a significant difference in the agreement for the two sets of experimental rotational strengths. That is, overall, the errors in calculated rotational strengths are significantly larger than the variations between the dispersive and FT rotational strengths. The agreement between calculated and experimental rotational strengths is at least as good as that for dipole strengths.

The quantitative agreement between calculated and experimental frequencies, dipole strengths, and rotational strengths strongly supports the reliability of the assignment of the fundamentals 9−56 of **1** arrived at from qualitative comparison of calculated and experimental absorption and VCD spectra.

Absorption and VCD spectra of **1** in CCl_4 solution in the C−H stretching region are shown in Figure 9. The absorption spectrum is shown at both 1 cm^{-1} resolution and at the resolution used in measuring the VCD spectra (Figure 9a,b). The VCD spectra of (+) and (−) enantiomers are shown individually (Figure 9c), together with the difference and sum spectra (Figure 9d,e). Again, artifacts do not contribute significantly to the spectra.

The frequencies, dipole strengths, and rotational strengths predicted for the C−H stretching modes using DFT, B3PW91 and B3LYP, and TZ2P are given in Table 1. Absorption and VCD spectra obtained thence are shown in Figure 10 together with the experimental spectra. There is considerable qualitative similarity between calculated and experimental spectra for both functionals and some features of the spectra can be plausibly assigned on the basis of the calculations. However, the spectrum comprises not only the 16 fundamentals of **1** but also overtone and combination bands, which in some cases will be in Fermi resonance with fundamentals. Given this complexity and the degree of resolution, we have not attempted a Lorentzian deconvolution.

The VCD spectrum of the C═C stretching mode of **1** (mode 56) was reported by Stephens and Clark.[5] The signal-to-noise was not large, but the sign of the VCD (positive for (*R*)-(+)-**1**) was clearly established. An anisotropy ratio of $\sim+3 \times 10^{-5}$

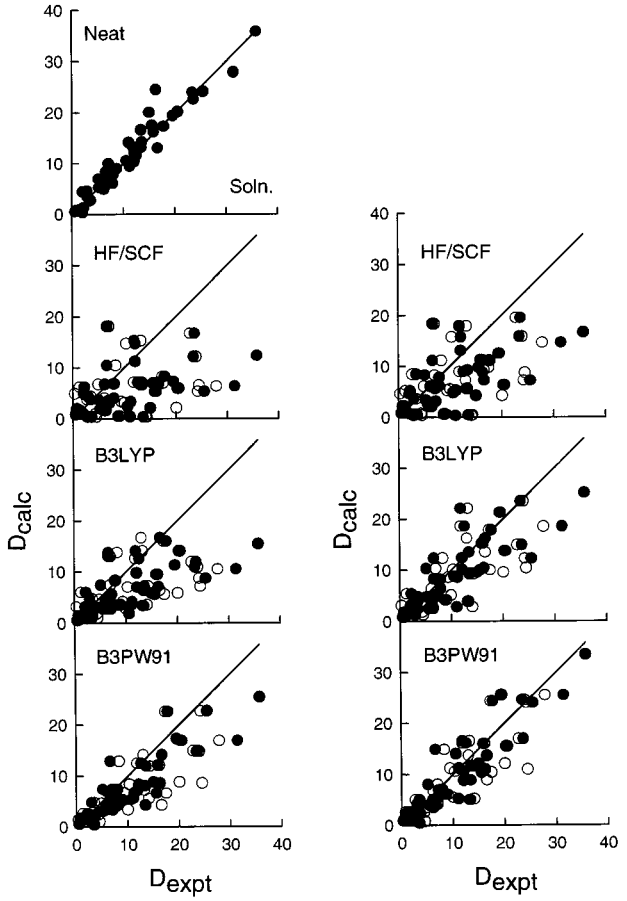

Figure 7. Comparison of calculated and experimental dipole strengths. Filled and open circles are for solution and neat liquid dipole strengths, respectively (Table 2), except in the top-most panel where they are plotted against each other. Mode 18 is off-scale, and, for the HF/SCF panels, mode 19 also). Left- and right-hand columns contain 6-31G* and TZ2P calculations, respectively. The straight lines are of unit slope.

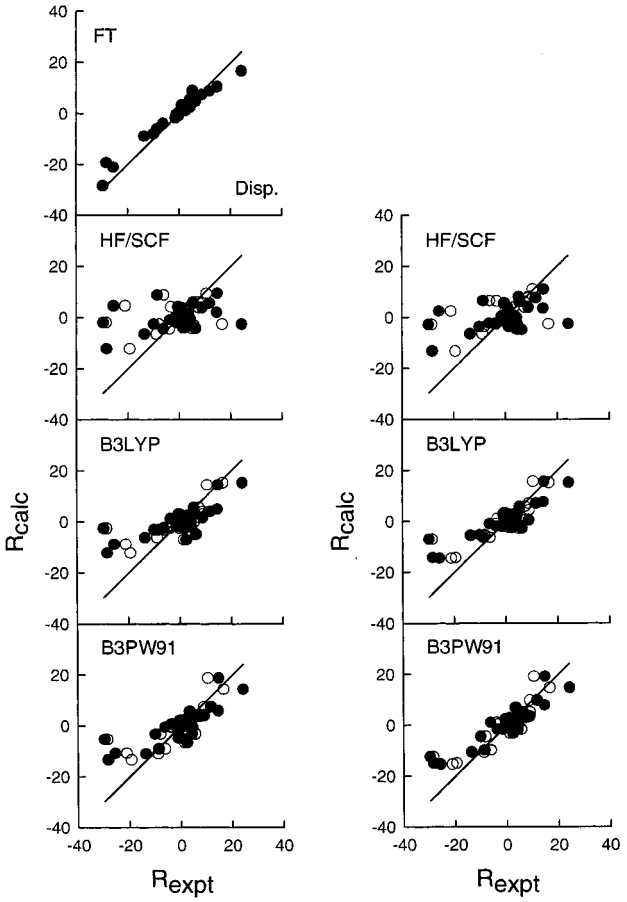

Figure 8. Comparison of calculated and experimental rotational strengths. Filled and open circles are for dispersive and FT rotational strengths, respectively (Table 2), except in the top-most panel where they are plotted against each other. Left- and right-hand columns contain 6-31G* and TZ2P calculations, respectively. The straight lines are of unit slope.

was reported. Our DFT/TZ2P calculations (Table 1) predict anisotropy ratios of $+8 \times 10^{-5}$, in satisfactory agreement with the experimental value given the uncertainty in the latter.

Absorption spectra of **1** at frequencies below 400 cm^{-1} have recently been reported by Polavarapu and Chen[53] (50−300 cm^{-1}, cyclohexane solution) and Polavarapu and Deng[54] (250−400 cm^{-1}, neat liquid). Bands assignable to fundamentals 1, 6, 7, and 8 are observed at ∼140, 260, 305, and 335 cm^{-1} respectively. Unresolved bands in the range 200−250 cm^{-1} can be attributed to modes 2−5. Polavarapu and co-workers have also investigated the VCD of **1** below 400 cm^{-1} [53,54] and reported evidence of VCD in the bands at ∼305 and 335 cm^{-1} due to modes 7 and 8. The two bands exhibit VCD of the same sign; unfortunately, the absolute sign was not established. The anisotropy ratios of both VCD signals were $\sim 3 \times 10^{-3}$. The DFT TZ2P calculations (Table 1) predict VCD intensities of the same sign with ansiotropy ratios in the range $(1-3) \times 10^{-4}$ for modes 7 and 8. At the present time, therefore, we cannot tell if our calculations correctly predict the VCD signs for modes 7 and 8, and the predicted anisotropy ratios are an order of magnitude lower than reported. Further studies of these signals are clearly necessary to establish whether or not they are artifactual in nature.

In addition to room-temperature, liquid-phase absorption, and VCD spectra, low-temperature spectra of matrix isolated **1** have also been reported.[7,14] The mid-IR absorption spectrum in an N_2 matrix over the range 800−1500 cm^{-1} displayed by Henderson and Polavarapu[14] does not exhibit significantly greater resolution of overlapping bands in comparison to the room temperature spectra (Figure 1). The corresponding VCD spectrum, in contrast, does show improved resolution compared to the room-temperature spectra in Figure 3, presumably due to the improved spectrometer resolution (1 cm^{-1}). Unfortunately, the signal-to-noise ratio of the VCD spectrum is very low, and only the largest VCD signals, originating in modes 27, 28, 31, 33, 34, 38, 41, and 43, can be regarded as unambiguous. Nevertheless, it does appear that modes 45−47 and 48−55 are significantly better resolved. In the case of modes 45−47 and 54−55 the low-temperature data are in agreement with the room-temperature spectra. In the case of modes 48−53, the opposite is true. It is also noteworthy that the VCD spectrum of modes 21−26 at low temperature shows little similarity to that at room temperature.

The C−H stretching absorption and VCD of **1**, matrix isolated in Ar, reported by Schlosser et al.[7] are dramatically more structured than the room-temperature spectra (Figure 9). These spectra demonstrate unequivocally the presence of a larger number of bands than attributable to fundamentals alone and confirm the wisdom of not attempting an analysis of this spectral region on the basis of harmonic calculations.

Frequencies, dipole strengths, and rotational strengths predicted using the B3PW91 and B3LYP functionals at the 6-31G* basis set level are given in Table 3. Absorption and VCD spectra predicted thence are shown in Figures 11 and 12. Overall, the spectra are very similar to those obtained at the TZ2P basis set level. The VCD spectrum is slightly more basis set dependent than the absorption spectrum. Comparison of the 6-31G* frequencies, dipole strengths, and rotational strengths

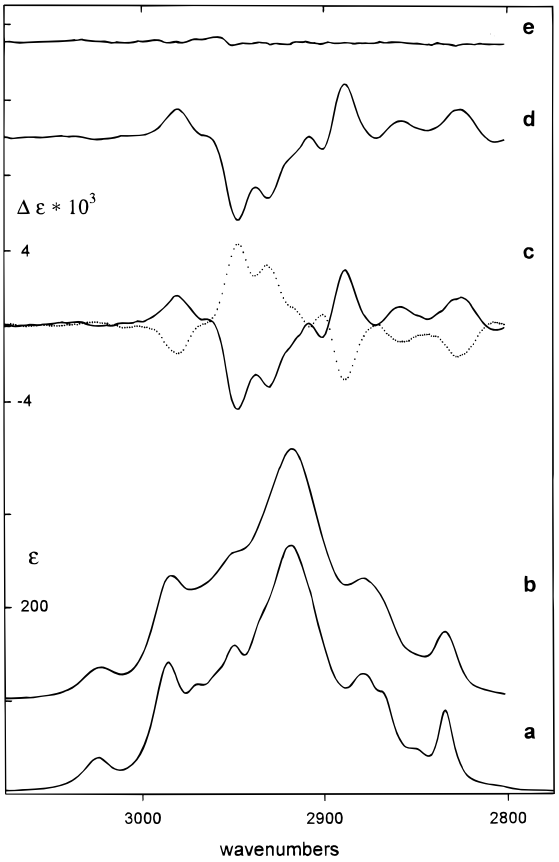

Figure 9. C−H stretching absorption (a and b) and VCD (c and d) spectra of **1** in CCl_4 solution (0.21M): (a) 3075−2775 cm^{-1}, resolution 1 cm^{-1}; (b) 3077−2801 cm^{-1}, resolution 11.0−9.6 cm^{-1}; (c) 3077−2801 cm^{-1}, resolution 11.0−9.6 cm^{-1}, (*R*)-(+)-**1** (solid line), (*S*)-(−)-**1** (dotted line); (d) VCD spectrum of (*R*)-(+)-**1** obtained from the spectra of (+)-**1** and (−)-**1** in (c); (e) "noise spectrum", the average of the spectra of (+)-**1** and (−)-**1** in (c). The VCD spectra in (c) are normalized to 100% ee.

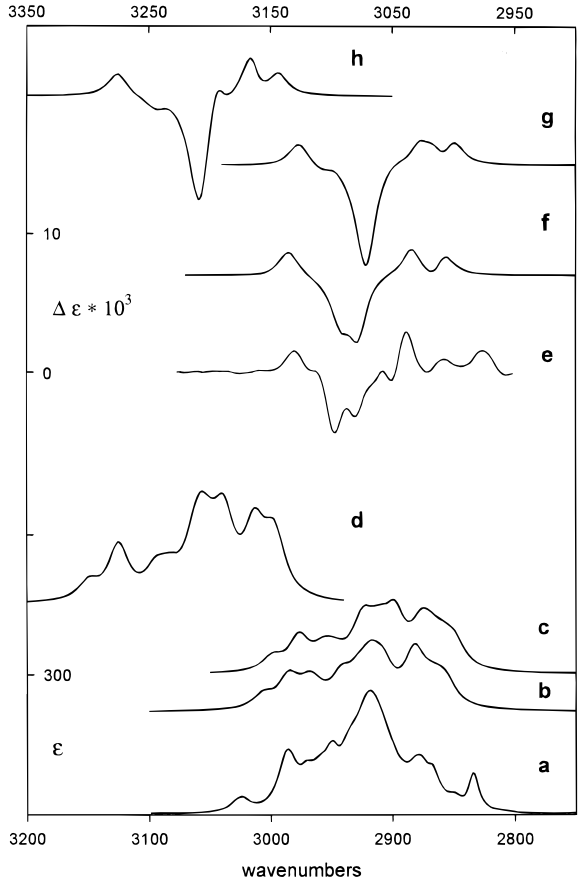

Figure 10. Experimental (a, e) and calculated (b−d, f−h) C−H stretching absorption (a−d) and VCD (e−h) spectra of (*R*)-(+)-**1**. The experimental spectra are from Figures 9a,d. Calculated spectra are (b, f) DFT/B3PW91/TZ2P; (c, g) DFT/B3LYP/TZ2P; (d, h) HF/SCF/TZ2P. $\gamma = 10$ cm^{-1} for all bands in b−d and f−h. The bottom and top scale apply to spectra a, e and b−d, f−h, respectively.

with experimental values is shown in Figures 6−8. As expected,[51] deviations of calculated frequencies are somewhat larger than for TZ2P frequencies (Figure 6). Calculated dipole strengths are on average lower than TZ2P dipole strengths and in somewhat worse agreement with experiment. For rotational strengths the changes with basis set are less systematic and do not significantly worsen the agreement with experiment.

In addition to DFT calculations, we have also carried out HF/SCF calculations at the TZ2P and 6-31G* basis set levels with the results given in Tables 1 and 3 and Figures 2, 4, 6−8, and 10−12. As with the DFT calculations, TZ2P and 6-31G* results are qualitatively similar. The HF/SCF spectra differ markedly from the DFT spectra and are in much worse agreement with experiment. The much lower accuracy of the HF/SCF frequencies, dipole strengths, and rotational strengths is also documented in Figures 6−8.

Discussion

VCD for **1** was first measured at USC using InSb detector based dispersive instrumentation. The C−H stretching region was studied; VCD was detectable, but the signal-to-noise ratio was low.[1] Subsequent improvements to this instrumentation, including the addition of a PbSnTe detector extended the low-frequency limit and permitted the observation of the VCD of the C═C stretch.[5] Interfacing of a matrix-isolation system to the dispersive VCD spectrometer permitted the measurement of C−H stretching VCD of Ar matrices of **1** at ∼18 K.[7] Under these conditions C−H stretching spectra are considerably more structured than in room-temperature liquid solution. Further development enhanced both the sensitivity and frequency range of the VCD instrument. Incorporation of a Si:As detector extended the low-frequency limit to ∼650 cm^{-1} and permitted measurement of the VCD of **1** in the range 750−800 cm^{-1}.[4] Addition of a HgCdTe detector shortly thereafter further enhanced sensitivity at frequencies above 800 cm^{-1} and permitted the mid-IR spectra over the range 1350−800 cm^{-1} reported here (Figure 3) to be measured. Addition of a new InSb detector also yielded higher sensitivity in the C−H stretching region, providing the new C−H stretching spectra reported here. Comparison of C−H stretching VCD spectra in Figure 9 to those reported previously[1,7] documents the dramatic improvement in instrumental sensitivity which has occurred since the mid-1970s.

The VCD of **1** has also been studied using dispersive instrumentation in other laboratories.[3,6,16] The C−H stretching spectrum was remeasured[6] with a signal-to-noise ratio similar to that of the earlier USC data.[1] Mid-IR spectra have since been reported by Keiderling[3] and Diem et al.[16] The spectrum of Keiderling over the frequency range 970−1250 cm^{-1} is qualitatively similar to the dispersive spectrum in Figure 3 over the same range. The signal-to-noise ratio is comparable; however, the resolution is considerably poorer. The spectrum of Diem et al.[16] covers the range 900−1400 cm^{-1}. While there are obvious similarities to the dispersive spectrum in Figure 3 over the same range, there are also substantial qualitative differences. In addition, when superimposed, there are major quantitative differences.

TABLE 3: 6-31G* Calculations for α-Pinene (1)[a]

	DFT								
	B3PW91			B3LYP			HF/SCF		
mode	*ν*	*D*	*R*	*ν*	*D*	*R*	*ν*	*D*	*R*
72	3173	35.5	−0.5	3162	38.4	−0.3	3338	39.2	−0.4
71	3158	26.5	3.9	3147	28.5	3.6	3318	37.2	2.2
70	3153	47.3	1.6	3141	53.0	1.7	3312	71.1	2.8
69	3139	42.0	1.6	3124	45.4	0.7	3285	52.4	−2.0
68	3133	27.9	−1.7	3116	30.9	−0.4	3274	39.7	0.0
67	3114	61.0	−10.3	3096	68.7	−9.3	3254	43.3	17.9
66	3106	7.2	0.1	3086	8.0	−0.2	3252	107.1	−36.8
65	3093	47.1	−8.6	3084	44.4	−11.6	3239	2.9	−5.0
64	3086	25.0	−0.7	3070	60.7	−0.2	3236	61.7	8.4
63	3082	63.5	0.5	3066	30.9	−0.7	3231	44.7	0.6
62	3071	72.1	−0.5	3058	84.6	0.7	3228	91.7	−1.7
61	3050	75.5	9.0	3042	72.1	6.7	3204	83.0	24.8
60	3047	29.7	−3.3	3035	23.6	−2.7	3203	52.9	−19.4
59	3045	21.3	2.2	3030	34.9	6.0	3193	20.8	0.8
58	3032	43.0	−3.1	3022	43.3	−3.2	3186	43.0	−3.9
57	3019	60.2	3.2	3008	62.8	3.3	3181	75.9	5.4
56	1746	2.3	0.9	1736	1.9	0.8	1893	3.7	1.0
55	1543	12.1	−0.4	1549	9.5	−0.1	1673	5.3	4.1
54	1536	14.8	0.1	1543	10.9	0.5	1666	12.1	−1.9
53	1521	5.6	1.5	1528	3.6	1.4	1649	0.4	0.4
52	1516	16.9	1.7	1523	10.5	1.2	1642	6.3	0.5
51	1514	4.3	−0.5	1520	6.4	0.0	1637	7.0	−0.1
50	1505	7.4	1.3	1513	7.4	1.5	1633	3.6	2.0
49	1502	22.7	−0.5	1508	8.7	1.9	1632	5.3	−1.1
48	1500	7.2	0.3	1508	14.1	−2.5	1624	15.3	−0.7
47	1439	17.3	−2.1	1448	11.3	−1.7	1574	7.2	−0.9
46	1435	5.4	−1.1	1442	1.9	−1.0	1567	2.4	−1.1
45	1422	25.4	−1.8	1430	15.4	−0.8	1557	12.3	−2.5
44	1384	4.7	−1.4	1384	4.6	−1.7	1510	6.7	0.2
43	1374	6.7	7.4	1372	4.2	4.1	1503	3.3	5.6
42	1354	2.0	1.4	1354	3.5	2.5	1479	0.4	−0.7
41	1315	8.8	−3.3	1311	5.8	−3.0	1443	2.1	−2.5
40	1288	0.5	−0.9	1290	0.5	−1.5	1407	0.8	−1.4
39	1264	12.5	−3.2	1262	12.6	0.0	1396	7.1	−3.1
38	1255	5.7	−5.3	1249	13.0	−2.6	1357	18.1	−2.0
37	1246	11.9	−6.5	1243	7.2	−7.0	1347	0.3	0.1
36	1220	7.4	4.4	1221	8.3	1.7	1331	6.8	3.9
35	1203	5.4	0.1	1200	3.6	−2.3	1299	0.5	−4.1
34	1162	14.1	14.3	1159	16.7	15.2	1257	6.7	−2.7
33	1140	8.4	−10.7	1139	7.0	−8.8	1246	14.7	4.6
32	1117	7.6	2.0	1116	9.8	3.1	1213	11.2	4.1
31	1090	7.2	−10.9	1092	5.6	−6.2	1186	3.4	−6.5
30	1074	6.9	3.7	1077	4.0	−4.9	1168	1.6	−4.2
29	1072	2.6	−4.9	1065	6.0	−0.6	1143	6.2	−2.0
28	1043	22.6	18.7	1045	16.0	14.5	1130	8.2	9.4
27	1030	1.6	−13.3	1033	1.5	−12.2	1115	2.0	−12.3
26	985	12.9	−9.0	982	13.8	−3.2	1067	10.4	8.7
25	978	8.1	2.5	981	3.4	1.2	1058	6.6	−0.7
24	962	1.7	−0.6	962	1.0	−2.4	1033	1.7	−4.5
23	956	4.1	5.6	948	3.5	2.7	1018	4.0	1.3
22	932	1.4	3.7	926	3.2	5.6	1000	4.9	6.0
21	911	14.9	−0.5	904	11.9	−2.0	974	16.7	−2.8
20	871	3.2	4.1	856	3.1	3.0	930	1.9	5.4
19	839	0.4	2.2	831	1.2	2.4	902	39.9	3.7
18	812	57.6	0.8	813	49.5	1.2	895	21.1	−1.0
17	790	16.9	5.9	783	14.1	5.0	843	5.9	2.0
16	679	0.4	0.3	675	0.3	0.4	723	0.1	−0.1
15	625	3.4	−5.9	626	2.8	−5.1	677	3.1	−5.0
14	575	6.6	3.4	574	5.6	2.6	624	6.9	3.0
13	486	4.8	−4.1	488	4.7	−3.6	519	4.3	−3.1
12	466	2.5	0.0	467	1.9	0.1	499	0.9	−0.5
11	426	8.6	0.4	429	7.1	0.2	465	6.5	0.2
10	394	3.5	0.1	397	2.7	0.2	426	2.2	0.1
9	388	1.0	0.4	390	1.0	0.7	421	0.4	0.7
8	331	17.8	−5.1	331	15.4	−4.3	364	11.0	−3.6
7	305	11.1	−6.7	305	11.4	−5.9	326	8.0	−4.5
6	261	1.1	1.9	263	1.1	1.5	279	0.6	0.5
5	230	3.4	4.1	229	2.4	3.4	245	2.8	3.8
4	204	4.6	−0.6	204	4.4	−0.4	214	2.2	0.8
3	194	1.6	−0.8	194	1.3	−0.7	206	0.9	−1.2
2	186	1.0	2.4	184	0.7	1.8	186	1.2	2.8
1	129	27.0	−2.0	129	22.1	−1.8	138	21.9	−2.3

[a] Units as in Table 1.

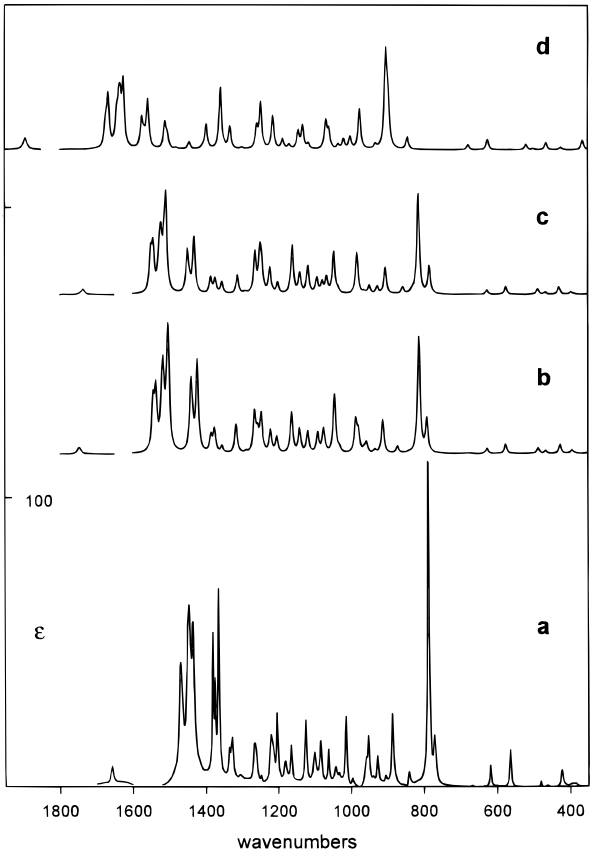

Figure 11. Experimental (a) and calculated (b−d) mid-IR absorption spectra of **1**. The experimental spectrum is from Figure 2. Calculated spectra are (b) DFT/B3PW91/6-31G*; (c) DFT/B3LYP/6-31G*; (d) HF/SCF/6-31G*. $\gamma = 4$ cm^{-1} for all bands in (b−d).

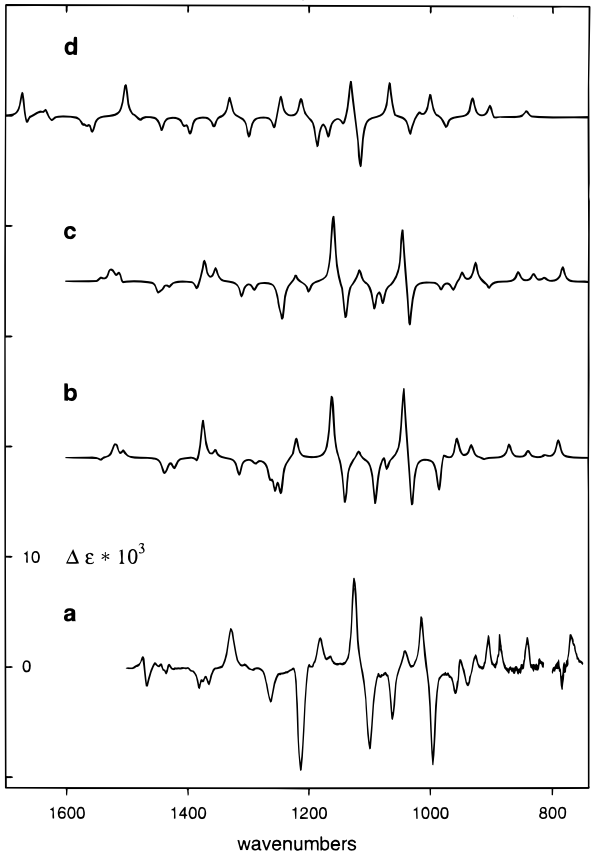

Figure 12. Experimental (a) and calculated (b−d) mid-IR VCD spectra of **1**. The experimental spectrum is from Figure 4. Calculated spectra are (b) DFT/B3PW91/6-31G*; (c) DFT/B3LYP/6-31G*; (d) HF/SCF/6-31G*. $\gamma = 4$ cm^{-1} for all bands in (b−d).

The application of Fourier transform (FT) methods to the measurement of VCD[2,3] has resulted in many mid-IR spectra of **1**. The first FT-VCD spectrum of **1**, covering the range 900−1350 cm^{-1}, was reported by Lipp et al.[8] Lipp and Nafie subsequently reported a spectrum for the range 810−1350 cm^{-1} of improved signal-to-noise ratio.[9] Significant differences were apparent from the earlier spectrum below 1000 cm^{-1}. Subsequent spectra from Nafie's laboratory[2,19,28,29] have not improved significantly on the earlier spectrum of Lipp and Nafie,[9] except that very recently the frequency range has been extended to include the region 1350−1500 cm^{-1}.[52] The FT VCD spectrum shown in Figure 3 exhibits the data from ref 2 together with the recent data at >1350 cm^{-1}.[52]

Mid-IR FT-VCD spectra of **1** have also been studied in other laboratories.[11−15,17,18,20−27,30] The highest signal-to-noise is exhibited by the recent spectra of Tsankov et al.[25] and Wang and Keiderling.[27] These spectra are qualitatively very similar to the best published spectra of Nafie and co-workers.[2,9,28,29] In a few studies the frequency range extended beyond the extremes of the 800−1350 cm^{-1} region. Polavarapu reported spectra over the ranges 1600−600 cm^{-1} [11] and 1350−750 cm^{-1},[18] respectively. Henderson and Polavarapu[14] also reported VCD spectra over the range 800−1500 cm^{-1}. The VCD spectra above 1350 cm^{-1} [11,14,21] are of considerably lower signal-to-noise than the spectrum in Figure 3.[52] Below 800 cm^{-1}, the spectra[11,18] differ markedly; the later data[18] are in agreement with the dispersive data shown in Figure 3 taken from ref 4. To date, there are no published FT-VCD spectra for the C═C and C−H stretching regions.

The majority of the mid-IR spectra reported have been obtained using neat **1**.[2,4,8−14,16,19,20,22,24,26,28,29] However, in some cases reported spectra were for CCl_4[21,25] or CS_2[3,15,17,18,23,27,30] solutions. Comparison of the recent FT-VCD spectra of Nafie[2,28,29] for the neat liquid, Tsankov et al.[25] for CCl_4 solutions, and Wang and Keiderling[27] for CS_2 solutions leads to the conclusion that, like the absorption spectrum, the VCD spectrum of **1** is insensitive to solvent and concentration, at least over the range 800−1350 cm^{-1}.

It is clear that the dispersive VCD spectra reported here are in excellent qualitative agreement with the best FT-VCD spectra, to the extent that they overlap in frequency range. In order to examine the quantitative agreement, we have compared our data to the FT VCD data of Nafie and co-workers.[9,52] Direct superposition (Figure 3) shows that the spectra are very similar. Some fraction of the difference can be attributed to differing resolution. To eliminate this contribution, we have also compared the rotational strengths obtained by Lorentzian fitting (Table 2). As seen in Figure 8, on average rotational strengths obtained from Nafie's spectra are somewhat (∼20%) smaller. This difference probably arises from differences in ΔA scale calibration, although some contribution from artifacts cannot be ruled out entirely.

We have utilized ab initio density functional theory to analyze the vibrational spectra of **1**. Recent advances in DFT methodology have made practicable the efficient calculation of HFFs, APTs, and AATs. Direct, analytical derivative methods are available for all three properties.[32,45,46] AATs can be calculated using GIAO basis sets.[32] In addition, the accuracy of density functionals has increased rapidly in recent years. In this work we have used hybrid density functionals,[47,55] which are currently the most accurate functionals available.[51,56−62] Specifically, we have used the B3PW91 functional of Becke[47] and the B3LYP variant.[42,43]

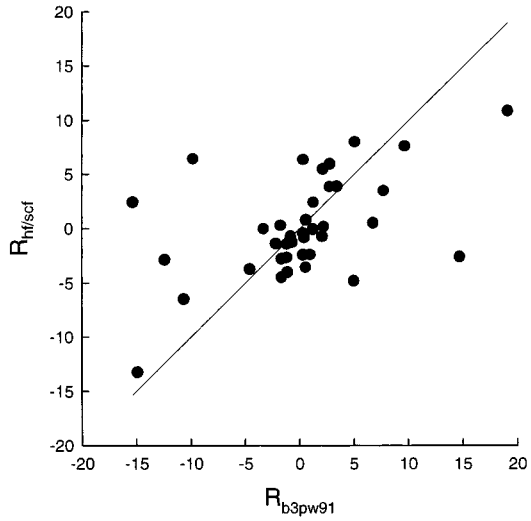

Figure 13. Comparison of HF/SCF and DFT/B3PW91 rotational strengths calculated at the TZ2P basis set level. The straight line is of unit slope.

Overall, DFT calculations of the absorption and VCD spectra of **1** using B3PW91 and B3LYP at the TZ2P basis set level are in sufficient agreement with the experimental spectra to provide a convincing assignment of a large majority of the fundamentals of **1**. The assignment is unambiguous for the fundamentals lying at frequencies below 1400 cm^{-1}. Spectra in the regions 1400−1500 and 2800−3100 cm^{-1} are more congested, and assignment is less straightforward. We have attempted a detailed analysis of the 1400−1500 cm^{-1} region, which includes fundamentals 48−55, while eschewing analysis of the highly complex C−H stretching region, 2800−3100 cm^{-1} , to which fundamentals 57−72 contribute.

The absorption spectra predicted using the B3PW91 and B3LYP functionals are qualitatively very similar and lead to identical assignments. Somewhat greater sensitivity to the choice of functional is exhibited by the VCD spectra. The difference is most noticeable for modes 21−25; the patterns of VCD intensities predicted by the two functionals are substantially different from each other and also from the experimental spectrum. The B3PW91 spectrum is somewhat closer to experiment. The VCD intensities predicted for modes 29 and 30 also differ significantly; here, the B3PW91 calculation is in agreement with experiment, while the B3LYP calculation is not. Overall, it is clear that the B3PW91 and B3LYP functionals are of very similar accuracy; to the extent that differences exist, B3PW91 appears to be a little superior to B3LYP.

We have also compared the TZ2P DFT calculations to HF/SCF calculations at the same basis set level in order to define the relative accuracies of the DFT and HF/SCF methodologies. HF/SCF absorption and VCD spectra are substantially different from the DFT spectra and in much worse agreement with experiment. The differences are especially apparent for the VCD spectra. The differential accuracy of DFT and HF/SCF is quantitated by comparison of predicted and experimental frequencies, dipole strengths, and rotational strengths. The percentage deviations of HF/SCF frequencies are much larger, and more variable, than for DFT frequencies. Dipole strengths and rotational strengths are in obviously worse agreement with experimental values. The differences in rotational strengths are further documented in Figure 13, where HF/SCF values are plotted versus DFT/B3PW91 values. The HF/SCF rotational strengths correlate with the DFT values very poorly with respect to both sign and magnitude. HF/SCF calculations do not, by definition, include (electron) correlation. DFT calculations do include correlation, and their accuracy depends only on the accuracy of the functional. It is by now well-known that with the B3PW91 and B3LYP functionals, DFT is substantially more accurate than HF/SCF. Our calculations for **1** further demonstrate the importance of this superior accuracy in predicting vibrational spectra.

The basis set dependence of our calculations has been examined by comparing results obtained using the 6-31G* and TZ2P basis sets. The much less complete basis set 6-31G* gives results in excellent qualitative agreement with the much larger TZ2P basis set.

The assignment of the spectra of **1** is not yet complete, and the agreement of theory and experiment is not perfect. Further matrix isolation studies of the absorption and VCD spectra would be useful in improving the assignment in the regions 1400−1500 and 2800−3100 cm^{-1}. The frequency range, instrumental resolution, and quantitative accuracy of the VCD spectrum all require improvement to yield more accurate values of rotational strengths for a larger number of fundamentals. Improved density functionals are needed to establish the degree to which remaining differences between calculated and experimental dipole and rotational strengths are due to residual errors in the harmonic calculations or, alternatively, to anharmonicity or solvent effects.

This work is an extension of prior studies of *trans*-oxirane-*2,3-d*$_2$[32] 6,8-dioxabicyclo[3.2.1]octane,[33] camphor, and fenchone[34,63] and further defines the reliability of DFT in predicting vibrational frequencies, dipole strengths, and rotational strengths. Additional work on a wider range of molecules is required to establish the generality of the conclusions resulting from the five molecules studied so far.

Conclusion

We have provided the first detailed theoretical analysis of the VCD spectrum of **1**. Our work has been made possible by the development of efficient techniques for the calculation of HFFs, APTs, and AATs using DFT. DFT now permits the prediction of VCD spectra of chiral molecules of substantial size with much greater accuracy and efficiency than has been practicable previously. Future developments, including functionals of yet higher accuracy than the current generation of hybrid functionals and the application of linear scaling methodologies, can be expected to further enhance the accuracy and efficiency of DFT calculations of VCD spectra.

Acknowledgment. We are grateful to Professor L. A. Nafie for allowing us to use unpublished VCD data from his laboratory. F.J.D. and P.J.S. also appreciate support from NSF, NIH, and SDSC over the years for our work on VCD, most recently from NIH Grant R01 GM51972.

References and Notes

(1) Nafie, L. A.; Keiderling, T. A.; Stephens, P. J. *J. Am. Chem. Soc.* **1976**, *98*, 2715.

(2) Nafie, L. A. In *Advances in Applied Fourier Transform Infrared Spectroscopy*; Mackenzie, M. W., Ed.; Wiley: New York, 1988; Chapter 3, p. 67.

(3) Keiderling, T. A. In *Practical Fourier Transform Infrared Spectroscopy*; Academic Press: New York, 1990; Chapter 5, p 203.

(4) Devlin, F.; Stephens, P. J. *Appl. Spectrosc.* **1987**, *41*, 1142.

(5) Stephens, P. J. and Clark, R. In *Optical Activity and Chiral Discrimination*; Mason, S. F., Ed.; Reidel: Dordrecht; 1979; p 263.

(6) Laux, L.; Pultz, V.; Abbate, S.; Havel, H. A.; Overend, J.; Moscowitz, A.; Lightner, D. A. *J. Am. Chem. Soc.* **1982**, *104*, 4276.

(7) Schlosser, D. W.; Devlin, F.; Jalkanen, K.; Stephens, P. J. *Chem. Phys. Lett.* **1982**, *88*, 286.

(8) Lipp, E. D.; Zimba, C. G.; Nafie, L. A. *Chem. Phys. Lett.* **1982**, *90*, 1.

(9) Lipp, E. D.; Nafie, L. A. *Appl. Spectrosc.* **1984**, *38*, 20.
(10) Nafie, L. A. In *Advances in Infrared and Raman Spectroscopy*, Clark, R. H. J.; Hester, R. E., Eds.; Wiley: New York, 1984; Vol. 11, Chapter 2, p 49.
(11) Polavarapu, P. L. *Appl. Spectrosc.* **1984**, *38*, 26.
(12) Polavarapu, P. L.; Michalska, D. F.; Back, D. M. *Appl. Spectrosc.* **1984**, *38*, 438.
(13) Polavarapu, P. L. In *Fourier Transform Infrared Spectroscopy*; Academic Press: New York, 1985; Vol. 4, Chapter 2, p 61.
(14) Henderson, D. O.; Polavarapu, P. L. *J. Am. Chem. Soc.* **1986**, *108*, 7110.
(15) Malon, P.; Keiderling, T. A. *Mikrochim. Acta.* **1988**, *II*, 279.
(16) Diem, M.; Roberts, G. M.; Lee, O.; Barlow, A. *Appl. Spectrosc.*, **1988**, *42*, 20.
(17) Malon, P.; Keiderling, T. A. *Appl. Spectrosc.*, **1988**, *42*, 32.
(18) Polavarapu, P. L. *Appl. Spectrosc.*, **1989**, *43*, 1295.
(19) Ragunathan, N.; Lee, N. S.; Freedman, T. B.; Nafie, L. A.; Tripp, C.; Buijs, H. *Appl. Spectrosc.*, **1990**, *44*, 5.
(20) Yoo, R. K.; Croatto, P. V.; Wang, B.; Keiderling, T. A. *Appl. Spectrosc.* **1991**, *2*, 231.
(21) Maurer, F.; Wieser, H. *SPIE* **1991**, *1575*, 410.
(22) Marcott, C.; Dowrey, A. E.; Noda, I. *Appl. Spectrosc.* **1993**, *47*, 1324.
(23) Chen, G. C.; Polavarapu, P. L.; Weibel, S. *Appl. Spectrosc.* **1994**, *48*, 1218.
(24) Polavarapu, P. L.; Chen, G. C.; Weibel, S. *Appl. Spectrosc.* **1994**, *48*, 1224.
(25) Tsankov, D.; Eggimann, T.; Wieser, H. *Appl. Spectrosc.* **1995**, *49*, 132.
(26) Niemeyer, M.; Hoffmann, G. G.; Schrader, B. *J. Mol. Struct.* **1995**, *349*, 451.
(27) Wang, B.; Keiderling, T. A. *Appl. Spectrosc.* **1995**, *49*, 1347.
(28) Nafie, L. A. *Appl. Spectrosc.* **1996**, *50*, 14A.
(29) Qu, X.; Lee, E.; Yu, G. S.; Freedman, T. B.; Nafie, L. A. *Appl. Spectrosc.* **1996**, *50*, 649.
(30) Malon, P.; Keiderling, T. A. *Appl. Spectrosc.* **1996**, *50*, 669.
(31) The one exception is ref 21.
(32) Cheeseman, J. R.; Frisch, M. J.; Devlin, F. J.; Stephens, P. J. *Chem. Phys. Lett.* **1996**, *252*, 211.
(33) Stephens, P. J.; Ashvar, C. S.; Devlin, F. J.; Cheeseman, J. R.; Frisch, M. J. *Mol. Phys.* **1996**, *89*, 579.
(34) Devlin, F. J.; Stephens, P. J.; Cheeseman, J. R.; Frisch, M. J. *J. Am. Chem. Soc.* **1996**, *118*, 6327.
(35) Brown, H. C.; Jadhav, P. K.; Desai, M. C. *J. Org. Chem.* **1982**, *47*, 4583.
(36) Kawiecki, R. W.; Devlin, F. J.; Stephens, P. J.; Amos, R. D.; Handy, N. C. *Chem. Phys. Lett.* **1988**, *145*, 411.
(37) Kawiecki, R. W.; Devlin, F. J.; Stephens, P. J.; Amos, R. D. *J. Phys. Chem.* **1981**, *95*, 9817.
(38) Stephens, P. J. *J. Phys. Chem.* **1985**, *89*, 748.
(39) Stephens, P. J. *J. Phys. Chem.* **1987**, *91*, 1712.
(40) Stephens, P. J.; Jalkanen, K. J.; Amos, R. D.; Lazzeretti, P.; Zanasi, R. *J. Phys. Chem.* **1990**, *94*, 1811.
(41) Frisch, M. J.; et al. *GAUSSIAN 95*, Development Version; Gaussian Inc.: Pittsburgh, PA, **1995**.
(42) Stephens, P. J.; Devlin, F. J.; Chabalowski, C. F.; Frisch, M. J. *J. Phys. Chem.* **1994**, *98*, 11623.
(43) Stephens, P. J.; Devlin, F. J.; Ashvar, C. S.; Chabalowski, C. F.; Frisch, M. J. *Faraday Discuss.* **1994**, *99*, 103.
(44) Bak, K. L.; Devlin, F. J.; Ashvar, C. S.; Taylor, P. R.; Frisch, M. J.; Stephens, P. J. *J. Phys. Chem.* **1995**, *99*, 14918.
(45) Johnson, B. G.; Frisch, M. J. *Chem. Phys. Lett.* **1993**, *216*, 133.
(46) Johnson, B. G.; Frisch, M. J. *J. Chem. Phys.* **1994**, *100*, 7429.
(47) Becke, A. D. *J. Chem. Phys.* **1993**, *98*, 5648.
(48) R. Ditchfield, *Mol. Phys.* **1974**, *27*, 789.
(49) Bak, K. L.; Jørgensen, P.; Helgaker, T.; Ruud, K.; Jensen, H. J. Aa. *J. Chem. Phys.* **1993**, *98*, 8873; **1994**, *100*, 6620.
(50) Hehre, W. J.; Schleyer, P. R.; Radom, L.; Pople, J. A. *Ab Initio Molecular Orbital Theory*; Wiley, New York, 1986.
(51) Finley, J. W.; Stephens, P. J.; *J. Mol. Struct. THEOCHEM* **1995**, *357*, 225.
(52) Nafie, L. A.; Long, F., private communication, 1997.
(53) Polavarapu, P. L.; Chen, G. C. *Appl. Spectrosc.* **1994**, *48*, 1410.
(54) Polavarapu, P. L.; Deng, Z. *Appl. Spectrosc.* **1996**, *50*, 686.
(55) Becke, A. D. *J. Chem. Phys.* **1993**, *98*, 1372.
(56) Wong, M. W. *Chem. Phys. Lett.* **1996**, *256*, 391.
(57) Scott, A. P.; Radom, L. *J. Phys. Chem.* **1996**, *100*, 16502.
(58) De Proft, F.; Martin, J. M. L.; Geerlings, P. *Chem. Phys. Lett.* **1996**, *250*, 393.
(59) Cheeseman, J. R.; Trucks, G. W.; Keith, T. A.; Frisch, M. J. *J. Chem. Phys.* **1996**, *104*, 5497.
(60) Foresman, J. B.; Frisch, A. E.; *Exploring Chemistry with Electronic Structure Methods*, 2nd ed.; Gaussian, Inc.: Pittsburgh, PA, 1996.
(61) Frisch, M. J.; Trucks, G. W.; Cheeseman, J. R. In *Recent Developments and Applications of Modern Density Functional Theory*, Seminario, J. M., Ed.; Elsevier: Amsterdam, 1996; Chapter 18, pp 679−707.
(62) Curtiss, L. A.; Raghavachari, K.; Redfern, P. C.; Pople, J. A. *J. Chem. Phys.* **1997**, *106*, 1063.
(63) Devlin, F. J.; Stephens, P. J.; Cheeseman, J. R.; Frisch, M. J. *J. Phys. Chem. A* **1997**, *101*, 6322.